The Volume Fraction of Crystalline Silicon in Semi-Insulating Polycrystalline Silicon (SIPOS)

B. Greenberg and T. Marshall

Philips Laboratories, North American Philips Corporation, Briarcliff Manor, New York 10510

ABSTRACT

The absolute volume of crystalline silicon in semi-insulating polycrystalline silicon (SIPOS) films was determined from x-ray powder diffraction measurements. The films, prepared by low pressure chemical vapor deposition (LPCVD), contained 20 or 27 atomic percent oxygen, and were annealed at 900°C for 30 min in dry nitrogen. Integrated intensities of the 111, 220, and 311 silicon lines were used together with corrections for preferred orientation to determine the crystalline volume. From a knowledge of the oxygen content of the films and their infrared absorption spectra the average oxidation state and volume of silicon oxide were estimated. The remaining volume was concluded to be amorphous silicon and was checked by independent experiments. A typical 1 μm thick film contains by volume 50 ± 4% crystalline silicon, 26 ± 5% oxide, and 24 ± 6% amorphous silicon. The effects of As^+ ion implantation and subsequent annealing are also described.

In order to understand electronic conduction mechanisms in SIPOS, a more detailed structural picture of the material is needed. Among the features still unknown are the amounts of crystalline silicon (c-Si) and amorphous silicon (a-Si) in films of this material, as well as the nature of the oxide. While transmission electron microscopy has provided information about the spatial distribution of c-Si, important questions remain about the distribution of oxide and a-Si. The studies cited below form, in large part, our picture of the SIPOS structure. They indicate the presence of discrete silicon and oxide phases, but they do not quantify the absolute content of c-Si or a-Si. For example, it is well known that SIPOS containing 25 atom percent (a/o) oxygen, when annealed at 900°C contains discrete Si and SiO_x phases (1, 2). Infrared absorption spectroscopy (3) indicates that the x in the SiO_x phase is approximately equal to 2. It is also known that if SIPOS containing 55-65 a/o oxygen is annealed below ≈ 1100°C, a silicon phase segregates, but does not fully crystallize (4, 5). This low silicon SIPOS is also known as silicon-rich oxide (SRO), and off-stoichiometric SiO_2. Finally Raman spectra characteristic of a mixture of c-Si and a-Si are seen in SIPOS containing 25 a/o oxygen after annealing at 900°C (6).

In the present study, x-ray powder diffraction was used to determine the volume of c-Si in the SIPOS films. This was done by comparing integrated intensity measurements from the films to those obtained from a series of calibration standards. These measurements also allowed us to numerically describe the degree of preferred orientation in the samples. The volume of oxide was calculated from a knowledge of the oxygen content and an estimate of the oxide composition. Oxygen content was determined by Rutherford backscattering (RBS) and an estimate of the oxide composition was based on both infrared absorption spectroscopy (IR) and x-ray photoelectron spectroscopy (XPS) (2, 7). The remaining volume is assumed to be amorphous silicon. Thus the volume fractions of c-Si, oxide, and a-Si sum to one

$$vf_{\text{c-Si}} + vf_{\text{oxide}} + vf_{\text{a-Si}} = 1$$

A check on the consistency of our results was made by measuring the c-Si content of various samples before and after high temperature anneals. Such anneals are expected to convert all a-Si to c-Si and SiO_x to SiO_2.

Experimental

SIPOS films were prepared by standard LPCVD procedures (8) from SiH_4 and N_2O at 650°C. Each sample was deposited on a 100-oriented Si substrate and then annealed at 900°C for 30 min in dry nitrogen. These films were our starting samples and were studied either before or after further processing. Table I shows sample processing information, oxygen content, and our estimate of x in SiO_x for the films studied. Some starting samples were subsequently As^+ ion implanted then examined. Doses ranged from 1×10^{15} to 6×10^{16} cm^{-2}, and energies of 100 or 200 keV were used. After implantation some samples were reannealed in dry nitrogen at either 900°C (samples S1, S3, and S5) or at 1150°C for 2.5h (sample S6). Starting sample S4 was studied with no additional processing, and sample S2 was studied after implantation, with no subsequent anneal.

The films were characterized in a variety of ways. X-ray powder diffraction was used to provide a qualitative survey of the samples, to measure preferred orientation, for quantitative c-Si determination, and to estimate crystallite size. Transmission electron microscopy (TEM) was used to determine the spatial distribution of c-Si, to measure film thickness, and to estimate crystallite size. In some samples film thickness was determined from optical measurements of angle lapped surfaces.

Three calibration standards (CS1-CS3) were prepared and used to establish the calibration curve shown in Fig. 1. This shows how the integrated intensity from silicon varies with the effective thickness of crystalline silicon. The calibration standards contain between 0.22 and 1.25 mg of crystalline silicon. The first calibration standard (CS1) was prepared by LPCVD of amorphous silicon and conversion to polycrystalline silicon by annealing at 800°C. This processing is sufficient to convert all the amorphous silicon to polycrystalline silicon (9). The thickness of this sample was determined from optical measurements of a 3.14° angle-lapped specimen. Calibration standards CS2 and CS3 were prepared by dusting silicon powder onto preweighed substrates, blowing off the excess material, and then reweighing. For each dusted sample the substrate was a glass slide coated with a thin layer of petroleum jelly in a 1 cm^2 area. The silicon powder used was National Bureau of Standards, SRM 640a. This material has a mean crystallite size of about 2 μm and was annealed in dry nitrogen at 900°C to relieve any strain due to previous grinding. Repeated weighing of the substrates before and after addition of the silicon indicated that the uncertainty

Table I. Description of samples where entries indicate: L, film prepared by LPCVD; A, anneal at 900°C for 30 min in dry N_2; A*, annealed at 1150°C for 2.5h in dry N_2;D, film prepared by technique of dusting 2 μm particles of crystalline silicon; a-Si, amorphous silicon; c-Si, crystalline silicon; *I(d, e)*, implanted with As^+ to a dose *d* ions cm^{-2} of energy *e*.

Label	Thickness or Weight	Preparation	Additional Processing	Oxygen atomic %	x
S1	0.14 μm	SIPOS, L,A	I(6 × 10^{15},100 keV),A	27.2(5)	1.7(2)
S2	0.95 μm	SIPOS, L,A	I(5 × 10^{15},100 keV)	20(2)	1.7(2)
S3	0.95 μm	SIPOS, L,A	I(5 × 10^{15},100 keV),A	20(2)	1.7(2)
S4	0.90 μm	SIPOS, L,A		20(2)	1.7(2)
S5	0.77 μm	SIPOS, L,A	I(1 × 10^{15},200 keV),A	20(2)	1.7(2)
S6	0.77 μm	SIPOS, L,A	I(1 × 10^{16},200 keV),A,A*	20(2)	2.0(0)
CS1	0.545 μm	a-Si, L	Anneal at 800° C	0	
CS2	0.490(25) mg	c-Si, D		0	
CS3	0.620(25) mg	c-Si, D		0	

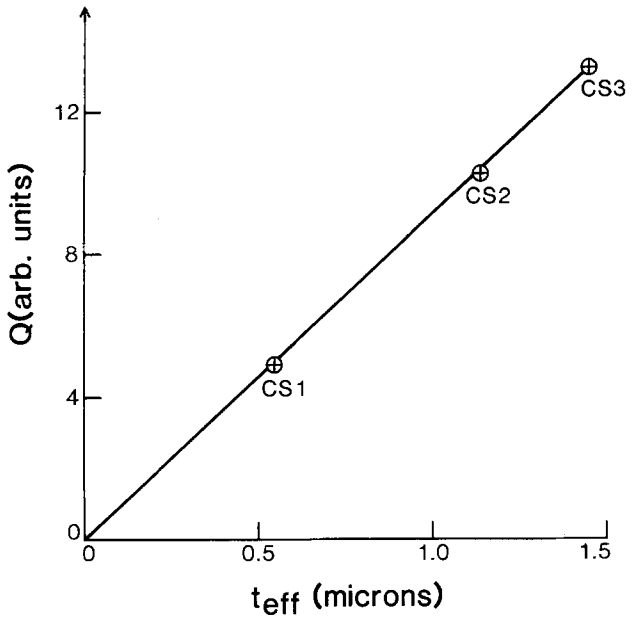

Fig. 1. Calibration curve showing variation in x-ray integrated intensity, Q, with effective thickness, t_{eff} of polycrystalline silicon.

in the silicon weight is between 0.02 and 0.03 mg. In the case of the dusted samples, an effective thickness was calculated by assuming that the known weight of silicon was spread uniformly over the 1.84 cm^2 area of irradiation and had bulk density, 2.328 g/cm^3.

For quantitative analysis the integrated intensity of the 111, 220, and 311 diffraction lines was measured using the Philips APD3700 x-ray powder diffractometer with associated quantitative scan software. Scans over silicon peaks were made at the rate of 20/0.02° step, and the angular range of the scans encompassed the full peak width. Figure 2 shows a survey scan of the calibration standard CS1, and Fig. 3 shows the survey scan of SIPOS sample S2. Scan ranges and background corrections are indicated.

Data Analysis

Some general features of the SIPOS films are illustrated by the data shown in Fig. 3, 4, and 5. These indicate that crystalline silicon is distributed as small crystallites throughout the annealed SIPOS film. In sample S2 the implantation of 5×10^{15} As^+ cm^{-2} causes the upper 0.14 μm region to become amorphous. A mean crystallite size of 35-45Å is indicated by the Scherrer broadening of the x-ray diffraction lines, and also by measurement of TEM high resolution and darkfield crystallite images. While the diffraction patterns show no obvious evidence of preformed orientation, quantitative intensity measurement indicates that all the SIPOS films have a more intense 111 and a weaker 311 than expected from a random sample.

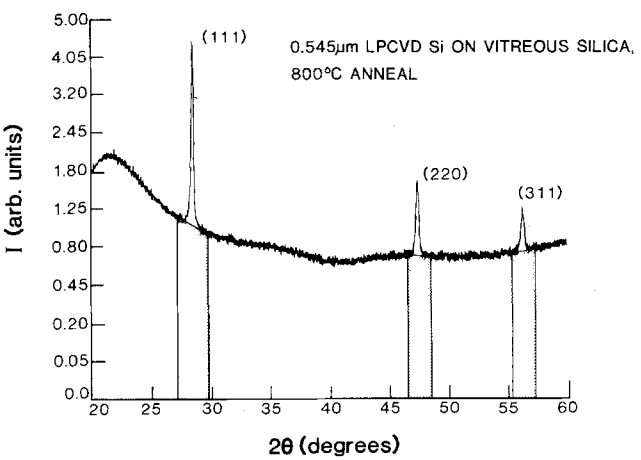

Fig. 2. X-ray diffractogram from calibration standard CS1 showing diffracted intensity I (a.u.) vs. diffraction angle 2θ. Angular regions used to establish integrated intensities are shown by vertical lines and background corrections are indicated by shaded areas.

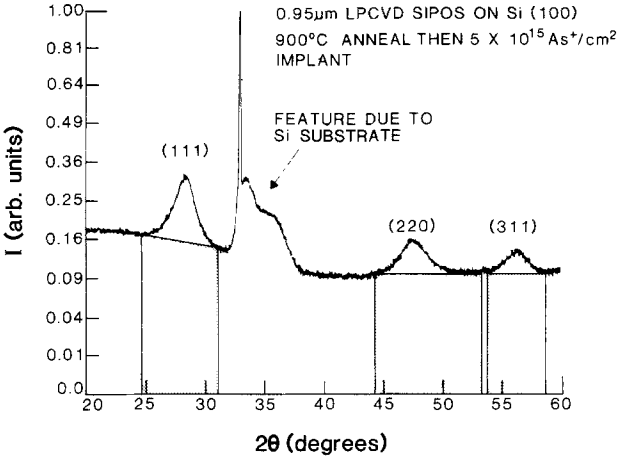

Fig. 3. X-ray diffractogram from SIPOS sample S2, showing diffracted intensity I (a.u.) vs. diffraction angle 2θ.

The procedure to perform a quantitative analysis on randomly oriented polycrystalline samples by x-ray powder diffraction is well established (10). It is based on the observation that integrated intensity of a diffraction peak from a given phase is proportional to the volume of that phase in a sample. For samples with preferred orientation, however, this proportionality does not hold, and it is in general necessary to account for preferred orientation. If the crystal structure of the phase is known, one can calculate values of the relative integrated intensity expected from a random sample. Using this information a quantitative analysis of a nonrandom sample can be performed by measuring the integrated intensity of a number of lines, and using the difference between measured and calculated relative intensities to correct for preferred orientation. This procedure has been described and used by Dixon (11) who defines both a texture parameter P_{hkl} and a summation of intensities, which we call Q. It is the quantity Q which is proportional to the volume fraction of a phase present in a sample with preferred orientation. For a single diffracting phase P_{hkl} can be written as P_i where

$$P_i = \frac{I_i/I_{c_i}}{Q}$$

and

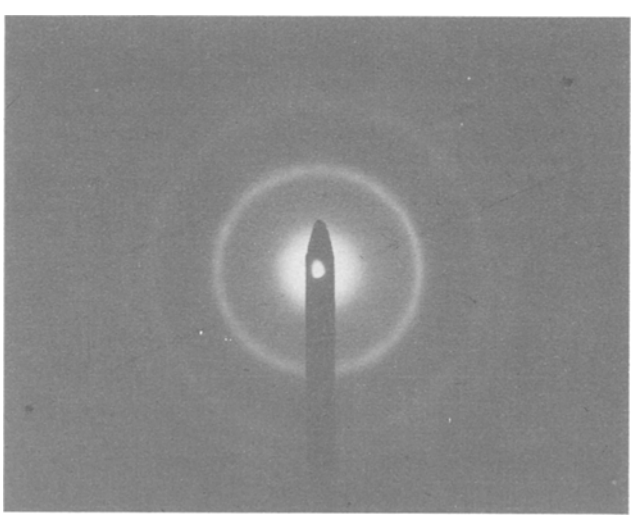

Fig. 4. TEM diffraction pattern of SIPOS in sample S2. Polycrystalline diffraction rings associated with scattering from 111, 220, and 311 planes of 35-40Å Si crystallites are seen. These correspond to the similarly indicated diffraction lines of Fig. 3.

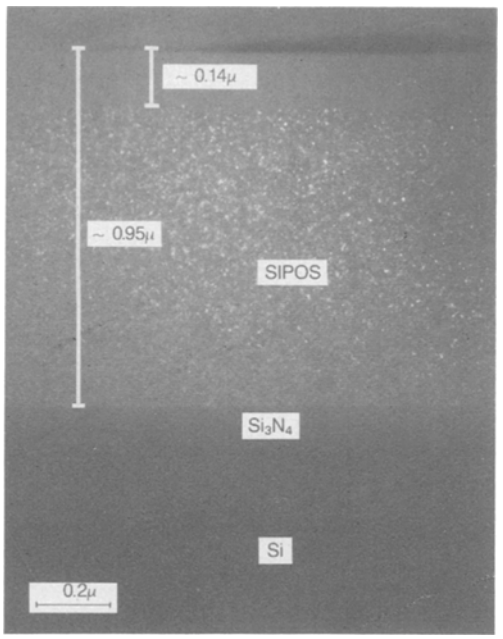

Fig. 5. Cross section TEM dark field micrograph of SIPOS sample S2 showing 0.95 μm of SIPOS. The upper 0.14 μm has been made amorphous by a 5×10^{15} cm^{-2} implant of 100 keV As$^+$ ions.

$$Q = \frac{1}{n} \sum_{i=1}^{n} I_i/I_{c_i}$$

In these expressions, I_i is the measured absolute integrated intensity of the ith diffraction line from the sample, n is the number of diffraction lines used to evaluate Q, and I_{c_i} is the calculated relative integrated intensity of the ith line is a perfectly random sample. In our analysis we have scaled $I_{c_{max}}$ to be 1.0 and determined I_{c_i} for the silicon 111, 220, and 311 reflections to be 1.000, 0.708, and 0.433. This calculation was made using the pertinent conditions of a thin sample on a diffractometer with a theta-compensating slit. The resulting value of Q, calculated as shown above, using experimental I_i's, is directly proportional to v_T, the total volume of crystalline silicon in the sample region studied. Thus $v_T = \kappa Q$ where κ is a constant which depends on details of the experimental setup, such as the x-ray generator power setting. Since all samples have the same effective area A, we have $v_T = t_{eff} A$ where t_{eff} is the effective thickness of the c-Si in the sample. Values of Q, t_{eff}, and P_i are given in Table II.

Results and Discussion

The results of this study are summarized in Table III, which shows the volume fraction (vf) of c-Si, oxide, and a-Si in each sample. The results for sample S2 are tabulated in two ways. In the first, the sample is labeled S2, and is considered to consist of the total film thickness, 0.95 μm as measured by TEM. In the second, the sample is labeled S2', and is considered to consist of only the 0.81 μm thick portion of S2 that was not implant amorphized. For sample S2, vf_{oxide} and $vf_{a\text{-}Si}$ are not well defined within the context of our analysis. However, sample S2' should be the same as our unimplanted sample, S4.

Table II. Diffraction data and results. t_{eff} (μm) is the effective thickness of a sample, Q is a weighted average of x-ray diffraction intensities and the P_{hkl}'s are texture parameters. t_{eff} for S1-S6 was obtained using the calibration curve in Fig. 1. Sources for other t_{eff}'s are described in the Experimental section of the text.

Sample	Q	t_{eff} (μm)	P_{111}	P_{220}	P_{311}
S1	786	0.087	1.3	1.1	0.6
S2	3749	0.414	1.4	0.9	0.7
S4	4038	0.446	1.4	0.9	0.7
S5	4005	0.442	1.3	0.9	0.8
S6	5766	0.636	1.2	0.9	0.9
CS1	4954	0.545	1.5	0.8	0.7
CS2	10,226	1.14	1.2	1.0	0.9
CS3	13,215	1.45	1.1	1.0	0.9

Table III. Summary of experimental results showing $vf_{c\text{-}Si}$, the volume fraction of crystalline silicon; vf_{oxide}, the volume fraction of silicon oxide [SiO_x, $x = 1.7(2)$]; and $vf_{a\text{-}Si}$, the volume fraction of amorphous silicon. These samples have undergone various LPCVD growth, anneal, and implant procedures. Row S2' refers to the 0.81 μm thick region of sample S2 that was not implant amorphized. Sample S1 contains 7 a/o As from intense implantation. EXAFS data on this sample indicate that the As is most likely associated with Si in an amorphous phase (16).

Sample	vf_{c-Si}	vf_{oxide}	vf_{a-Si}
S1	0.62(6)	0.34(5)	0.04(8)
S2	0.44(4)		
S2'	0.50(4)	0.26(5)	0.24(6)
S4	0.50(4)	0.26(5)	0.24(6)
S5	0.57(4)	0.26(5)	0.16(6)
S6	0.83(4)	0.24(5)	0

Based on repeated measurements, we estimate the experimental uncertainty when comparing $vf_{c\text{-}Si}$'s to be ±0.01 for samples S2-S6 and ±0.04 for S1 which was much thinner than the others and which showed larger statistical fluctuation in repeated measurements of diffraction intensities. The uncertainties shown in Table III are in the absolute values of the $vf_{c\text{-}Si}$'s. The primary reason for their larger values comes from a systematic error introduced by approximating the nonlinear background beneath the relatively broad SIPOS peaks by a sloping linear background correction.

Sample S4, which was not implanted, consists of a 0.90 μm SIPOS sample containing 20 ± 2% oxygen as determined by RBS. It was studied after annealing at 900°C for 30 min in dry nitrogen. X-ray diffraction indicates that this sample contains a $vf_{c\text{-}Si}$ of 0.50 ± 0.01. Because of the potential systematic error mentioned above, we estimate that $vf_{c\text{-}Si} = 0.50 \pm 0.04$ in absolute terms. This is what we list in Table III.

The oxide content of sample S4 is estimated to be 0.26 ± 0.05 vf. To obtain this number we need to know the oxygen content of the film, the average oxidation state, or composition of the oxide, and its density. The oxide composition was estimated by two independent procedures. In the first, we measured the position of the predominant IR absorption peak near 1060 cm^{-1} from our SIPOS and compared this with the position of the Si-O stretching peaks in the data of Schumann *et al* (12). They measured this peak position for a set of SiO_x films where x was known. We determined the value of x in our films by comparison to these data. In the second, we used the published raw XPS data of Thomas and Goodman (2) (taken on samples very similar to our S4) to estimate x. Following Adachi and Helms (7), we interpreted the spectra as due mainly to Si^0 and Si^{4+}. Both techniques yield $x = 1.7$, and we estimate the uncertainty in x to be ± 0.2. The density of oxide is assumed to be 2.2 g/cm^3. To obtain the oxide content of the film we use the expression

$$vf_{oxide} = \left[1 + \frac{\rho_{ox} M_{Si}}{\rho_{Si} M_{ox}} \left(\frac{x}{y} - x - 1\right)\right]^{-1}$$

This is a generalization of Eq. [1] of Ni and Arnold (13) and allows vf_{oxide} (their v_2) to be calculated knowing x, the oxide stoichiometry; y, the atomic fraction of oxygen in

the film; ρ_{Si} and ρ_{ox}, the densities, and M_{Si} and M_{ox}, the molecular weights of Si and SiO_x.

The volume fraction of amorphous silicon, $vf_{a\text{-}Si}$ was then determined from our working assumption

$$vf_{c\text{-}Si} + vf_{oxide} + vf_{a\text{-}Si} = 1$$

We obtain $vf_{a\text{-}Si} = 0.24 \pm 0.06$ in sample S4, or that 24% of the sample volume is amorphous silicon. Our estimate of $vf_{oxide} + vf_{a\text{-}Si}$ was checked in another series of experiments in which $vf_{c\text{-}Si}$ was measured in sample similar to S4 before and after an 1150°C, 2.5h anneal in dry nitrogen. Such an anneal is expected to convert all the SiO_x to SiO_2 and to convert all the a-Si to c-Si. This should increase $vf_{c\text{-}Si}$ to 0.74 from 0.50, a ratio of 1.48. We have checked this by determining the ratio of $vf_{c\text{-}Si}$ in sample S6 to that in S5. Experimentally we observe

$$\frac{vf_{c\text{-}Si}\,(S6)}{vf_{c\text{-}Si}\,(S5)} = 1.46$$

which agrees within experimental error with the results predicted from S4.

Effects of arsenic implantation are seen by comparing samples S2 and S4. These samples are similar except that after annealing S2 was arsenic implanted at 100 keV with a dose of 5×10^{15} As^+ cm^{-2}. A TEM micrograph of this sample (Fig. 5) indicates no observable c-Si in the top 0.14 μm implant-damaged region. The c-Si which was observed in this region before implantation has been made amorphous by the implant. We would expect a decrease in $vf_{c\text{-}Si}$ for S2 (as compared to S4) of 0.14 μ/0.95μ, or 15%. Within experimental error this is what was measured: $vf_{c\text{-}Si}$ in S2 is 0.44 ± 0.01 —down by 12% from that seen in S4. For S2' (the unaffected region), we obtain $vf_{c\text{-}Si}$ vf_{oxide}, and $vf_{a\text{-}Si}$ values identical to those of S4.

Effects of reannealing arsenic-implanted samples are seen in samples S1, S3, and S5, which were reannealed at 900°C for 30 min. Our results show that after implantation plus reannealing two things occur: first c-Si is reformed in the amorphous region (see Fig. 6), and second, more c-Si is present than existed before implantation. Sample S5 (which TEM indicates was amorphized to one-third its depth by the 200 keV implant) contains 0.57 $vf_{c\text{-}Si}$ after reannealing. This is a 14% increase over nonimplanted samples S4 and S2', and results in a calculated decrease of 33% in $vf_{a\text{-}Si}$. This is consistent with all the a-Si in the implanted region crystallizing during the 900°C 30 min reannealing process. Sample S1, which is only 0.14 μm thick, contains 0.62 $vf_{c\text{-}Si}$ after a heavy implant and reanneal. This sample was "amorphized" throughout its depth by the implant. The calculated $vf_{a\text{-}Si}$ in this sample after reannealing is 0.04 ± 0.08, which is consistent with a complete lack of a-Si. We think that the quantity of c-Si in these samples is much greater than what would be seen if an unimplanted sample were just reannealed for an additional 1/2 hour at 900°C without implantation. In other words we think that the ion implantation is responsible for the additional crystallization.

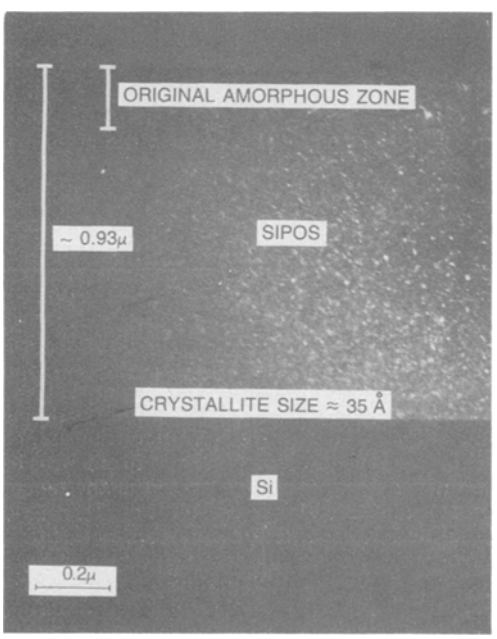

Fig. 6. Cross-section TEM dark field micrograph of SIPOS sample S3. Like S2, this sample was implanted with 5×10^{15} cm^{-2} As^+ at 100 keV. The sample was subsequently annealed, causing silicon in the implant-amorphized region to recrystallize.

A model of SIPOS has been proposed by Olego and Baumgart (6) which is based on Raman scattering data and places the a-Si in SIPOS on the surface of silicon crystallites. The $vf_{a\text{-}Si}$ we measure (0.24 ± 0.06 in sample S4) corresponds closely to the percentage of silicon atoms which are surface atoms in our ~ 40Å diam crystallites (*e.g.*, 21 a/o of silicon atoms are surface atoms in a cubic crystallite of size $6 \times 6 \times 6$ unit cells). It may therefore be the case that the a-Si we report is just this surface layer. In this case the x-ray results indicate that the surface atoms clearly do not lie on the continuation of the c-Si structure.

Finally we note that the diffraction feature that occurs between 31° and 38° in our Fig. 3 is due to the 100 oriented single-crystal silicon substrate. Analogous features seen by Prasad *et al.* (15) are almost certainly due to their 111 oriented silicon substrate and not to an anomalous form of silicon in the SIPOS. In addition it is likely that the features they labeled as SiO in their diffractograms are diffraction of CuK_β radiation by the substrate (333) and (444).

Conclusion

We have measured the quantity of polycrystalline silicon in various annealed and implanted SIPOS films. Typical unimplanted films which contain 20 a/o oxygen and which were annealed for 30 min contain $50 \pm 4\%$ by volume crystalline silicon. They contain $26 \pm 5\%$ SiO_x (with $x = 1.7 \pm 0.2$), and the remaining $24 \pm 6\%$ is amorphous silicon. We have demonstrated that As^+ implantation destroys the crystalline silicon structure in the implanted region, and that subsequent annealing restores the crystalline structure and results is a noticeable increase in the volume of crystalline silicon over the preimplantation value.

Acknowledgments

We wish to thank M. Kaczenski for help with the x-ray work, and J. Petruzzello and O. Hellman for TEM work and useful discussions. In addition, we wish to thank Dr. A. E. T. Kuiper for RBS analysis of one of our samples and S. Ueland and the staff of the Philips Laboratories clean room for special processing.

Manuscript submitted Aug. 30, 1987, revised manuscript received Feb. 17, 1988.

Philips Laboratories assisted in meeting the publication costs of this article.

REFERENCES

1. M. Hamasaki, T. Adachi, S. Wakayama, and M. Kiuchi, *J. Appl. Phys.*, **49,** 3987 (1978).
2. J. H. Thomas and A. M. Goodman, *This Journal,* **126,** 1766 (1979).
3. H. R. Maxwell, Jr. and W. R. Knolle, *ibid.,* **128,** 576 (1981).
4. A. Hartstein, J. C. Tsang, D. J. DiMaria, and D. W. Wong, *Appl. Phys. Lett.,* **36,** 836 (1980).
5. J. D. DiMaria, D. W. Dong, C. Falcony, T. N. Theis, J. R. Kirtley, J. C. Tsang, D. R. Young, and F. L. Pesavento, *J. Appl. Phys.,* **54,** 5801 (1983).
6. D. Olego and H. Baumgart, *Bull. Am. Phys. Soc.,* **32,** 652 (1987), and *J. Appl. Phys.,* In press (1988).
7. T. Adachi and C. R. Helms, *This Journal,* **127,** 1617 (1980).
8. M. L. Hitchman and J. Kane, *J. Cryst. Growth,* **55,** 485 (1981).
9. A. Martinez, Private communication.
10. H. P. Klug and L. E. Alexander, "X-ray Diffraction Procedures," John Wiley and Sons, Inc., New York (1970).

11. M. J. Dixon, *J. Appl. Crystallogr.*, **2,** 176 (1969).
12. L. Schumann, A. Lehmann, H. Sobotta, V. Riede, U. Teschner, and K. Hubner, *Phys. Status Solidi B*, **110,** K69 (1982).
13. J. Ni and E. Arnold, *Appl. Phys. Lett.*, **39,** 554 (1981).
14. L. A. Nesbit, *ibid.*, **46,** 38 (1985).
15. R. V. Prasad, F. A. Selim, and D. D. L. Chung, *Mater. Lett.*, **4,** 71 (1986).
16. E. Canova, Y. H. Kao, T. Marshall, and E. Arnold, To be published.

Nodule Formation in Electroless Copper Baths

R. Junginger

IBM, Deutschland, German Manufacturing Technology Center, 7032 Sendelfingen, Germany

ABSTRACT

The formation rate of copper nodules in electroless copper baths, which is a measure of the bath stability, was studied by means of a nodule monitoring technique as a function of the presence of complexing agents for copper (I)-ions and of dissolved oxygen both in the presence and absence of surfactant. In the presence of dissolved oxygen the stabilizing effect of complexing agents including cyanide is relatively small and does not correlate with the formation constants of the respective Cu(I)-complexes. In absence of oxygen, significant stabilization is exerted by cyanide and phenanthroline-(1,10), but not by the other investigated complexing agents. Dissolved oxygen dramatically reduces the rate of nodule formation. Bubbling of air through the bath instead of nitrogen reduces the density of nodules deposited on the monitors by more than four decades both in the presence and absence of complexing agents. This effect is further enhanced by increasing the oxygen content of the bubbled gas mixture up to 50%. The bath does not become passive, if the concentration of formaldehyde is sufficiently high. These findings support a nodule formation model in which the bivalent copper complex is adsorbed on extraneous germs, then reduced by formaldehyde in a two-electron step to adsorbed metallic nuclei which subsequently grow to nodules. Oxygen stabilizes through reoxidation of nuclei, whereas cyanide and phenanthroline-(1,10) in absence of oxygen may inhibit either adsorption or onset of growth. A mechanism via monovalent copper intermediate is excluded.

Electroless plating baths are known to deposit metal not only on the catalytic surface regions of the substrates, but also to some extent on nonactivated regions and on the surface of the plating equipment. This tendency basically results from the metastable thermodynamic character of electroless baths, *i.e.*, the reducing agent is present everywhere in the bulk of the baths, where any catalytic germ may be sufficient to initiate metal nucleation, whereas in electroplating processes the reducing power provided by electric current is located selectively at the metal surfaces to be plated.

In electroless copper plating the produced extraneous copper is deposited in form of individual and aggregated spherical particles, so-called nodules. While plating lines and through-holes of printed circuit boards these particles settle down also at the boundaries between plated copper and photoresist, where they become a source of defects during succeeding process steps.

The tendency to form extraneous copper is generally denoted instability. Stable baths ideally would not deposit extraneous copper at all. However, completely stable baths do not exist and the term "stable bath" implies a tendency to deposit extraneous copper to a relatively low extent rather than absolute absence of extraneous copper formation.

To enhance bath stability, various additives are applied as stabilizers in commercial baths (1-4). The generally accepted theory of stabilization as exerted by additives was reviewed by Ehrich (5). It postulates a one-electron reduction of Cu(II) to Cu(I) in the bulk of the bath. In the alkaline bath environment Cu(I) precipitates as cuprous oxide which disproportionates to Cu(II) and Cu(0)-nuclei. These nuclei are told to be the growth centers for the formation of nodules. Oxygen is said to disturb this reaction sequence by reoxidizing Cu(I) to Cu(II), whereas cyanide is supposed to destroy Cu(I) by complexation. Thus, both agents are said to suppress nodule formation by adversely affecting the steady-state concentration of Cu(I)-intermediate. So far, there seems to be no proof for this mechanism nor any accepted model for details of the nodule nucleation reaction sequence, *e.g.*, concerning the role of particles as nucleation centers.

The initial concept of this work was to test the Cu(I)-complexation model by adding to the bath a series of complexing agents for Cu(I)-ions with complex stability constants covering a range of over 20 decades, as complexing agents had been supposed to be the main stabilizers. The complexing agents were applied individually as well as in combination with one or both of air and a surfactant. In a second series of experiments the oxygen content of the bubbled oxygen/nitrogen mixture was varied between 21 and 100%. As a first step, however, a method for quantitative characterization of bath stability had to be developed.

Experimental

All experiments were made at elevated temperature with electroless copper plating baths containing copper sulfate, EDTA, formaldehyde, and sodium hydroxide as major components. Surfactant, complexing agents for copper(I)-ions and dissolved oxygen were optionally applied as minor constituents. The concentration of formaldehyde was varied between 12 and 300% of the standard value in order to keep the nodule count within the limits set by the monitoring method used. Complexing agents were applied at 0.0002 mol/liter. The concentration of dissolved oxygen was varied by varying the composition of bubbled oxygen/nitrogen mixtures.

To characterize bath stability a nodule monitoring technique was developed. Bath samples of 500 ml were sucked through a filter having pores of 0.8 μm nominal width and subsequently applied for plating. All experiments were made at clean room conditions in a thermostated beaker bath. Standard duration of all runs was 5h. The bath composition was controlled by manual *p*H analysis and NaOH and formaldehyde replenishments in intervals of 1h. The plating rate was controlled by the mass increase of copper-coated epoxy coupons. The mixed potentials was measured at a copper wire *vs.* a Ag/AgCl electrode and continuously recorded. An alumina coupon of 10 cm^2 area having a defined surface roughness was placed in the beaker horizontally about 2 cm above the bottom. During plating, nodules settled down onto the upper surface of that monitor. After finishing a plating run the coupon was carefully removed from the bath. The number of nodules sedimented on the upper surface of the monitor was counted either by means of optical microscopy or by SEM, depending on size and density of the nodules. The size distribution was determined by an automatic image processing system. On the lower surface of the monitor generally no nodules were found.